ISSN 0031-918X, The Physics of Metals and Metallography, 2013, Vol. 114, No. 11, pp. 885–892. © Pleiades Publishing, Ltd., 2013.
Original Russian Text © M.V. Petrik, O.I. Gorbatov, Yu.N. Gornostyrev, 2013, published in Fizika Metallov i Metallovedenie, 2013, Vol. 114, No. 11, pp. 963–970.

THEORY OF METALS

Effect of Magnetism on the Solution Energy of 3*p* (Al, Si) and 4*p* (Ga, Ge) Elements in Iron

M. V. Petrik[a, b], O. I. Gorbatov[b], and Yu. N. Gornostyrev[b, c]

[a] *Ural Federal University, ul. Mira 19, Ekaterinburg, 620002 Russia*
[b] *Institute of Quantum Materials Science, ul. Bazhova 51, Ekaterinburg, 620107 Russia*
[c] *Institute of Metal Physics, Ural Division, Russian Academy of Sciences, ul. S. Kovalevskoi 18, Ekaterinburg, 620990 Russia*
e-mail: Mikhail.Petrik@iqms.ru

Received March 26, 2013

Abstract—The method based on the density-functional theory has been used to study the solubility of 3*p* (Al, Si) and 4*p* (Ga, Ge) elements in ferromagnetic and paramagnetic states of bcc iron. To simulate the paramagnetic state, two different approaches have been employed, which were implemented using the SIESTA and LSGF packages. It has been established that the solution energy of all these impurities decreases upon the transition into the paramagnetic state. The solution energies obtained by averaging over the ensemble of unpolarized magnetic configurations agree well with the values obtained in the coherent-potential approximation. At the same time, the allowance for the magnetic polarization in the vicinity of an impurity leads to a decrease in the solution energy, which is most clearly pronounced at temperatures close to T_C. The temperature dependence of the solution energies of the impurities in the paramagnetic state is discussed.

Keywords: soft magnetic materials, iron alloys, paramagnetic state, first-principles calculations, solubility of impurities

DOI: 10.1134/S0031918X13110094

1. INTRODUCTION

Fe–*X* (*X* = Al, Si, Ga, Ge) alloys based on bcc iron with concentrations of the alloying elements close to the boundary of the two-phase field are of great interest in light of their unusual magnetic properties. The soft magnetic alloys Fe–Si and Fe–Al find wide application due to the high values of their magnetic susceptibility and high saturation magnetization. Their magnetic properties can be significantly improved by heat treatment in a dc magnetic field or under a mechanical load, which leads to enhanced magnetic anisotropy [1–4] (induced magnetic anisotropy). At the same time in the Fe–Ga and Fe–Ge alloys, in which alloying is accompanied by a significant increase in the magnetostriction [5–7], the application of an external load does not exert a significant effect on the magnetic anisotropy.

According to the existing concepts [4, 8 –10], both the induced magnetic anisotropy and the large magnetostriction of these alloys are due to a specific structural state that is characterized by the existence of a short-range order of the *B*2 type. However, the origin of such short-range order is still under discussion (in particular, the phase with a superstructure of the *B*2 type is absent at all in the phase diagrams of the Fe–Ga and Fe–Ge alloys below T_C). As was shown in [3] for Fe–Si, ferromagnetic state calculations do not shed light on the *B*2 type short range order formation at small Si concentrations. It has been shown in [4] that this type of short-range order can exist in the paramagnetic state of the Fe–Si alloy and can be inherited upon quenching. Thus, to understand processes of the formation of short-range order in these alloys, the investigation of the behavior of the alloying elements in various magnetic states of the bcc iron is required.

The behavior of impurities in bcc iron has been studied theoretically in numerous works [11–14], in which, as a rule, the calculations were performed for the case of a completely magnetically ordered (ferromagnetic) state. At the same time, in the region of technologically important temperatures the magnetic state of bcc iron is partly or completely disordered. The available experimental data clearly indicate a significant effect of magnetism on the processes of solid-solution decomposition, precipitation, and ordering [15, 16]. The important role of magnetism in the thermodynamics of iron and its alloys was already noted in the classical works of 1960–1980s [17–20]. Therefore, the consistent description of iron alloys requires a transition onto a microscopic level with allowance for the electronic structure and magnetic state. This approach has been realized in recent works [4, 9, 10, 22–24], where

the impact of magnetism on the solubility of alloying elements and phase equilibrium has been shown.

The paramagnetic (PM) state calculation is a complex problem in the modern physics of solids. There exist several approaches to its solution, which are based, e.g., on a temporal averaging of single-site states (dynamic mean-field theory (DMFT) [25, 26]), on the approximation of disordered local magnetic moments (DLM) [27–29], or approximation of paramagnetic state as a superposition of spin waves [30]. The DMFT method consistently takes into account the effect of the temperature and electron–electron correlations; however, to calculate the solution energy of an impurity, one must use a large supercell, which makes this method too cumbersome. The DLM approach is widely used to simulate the paramagnetic state in terms of the coherent-potential approximation (CPA), in which it is assumed that there is a 50% probability that the magnetic atom at a site is in the state with a spin up and with the same probability in the state with a spin down. In terms of the CPA, the calculation of the total energy of the alloy in the paramagnetic state is not a complicated problem, but the approximations used in this approach do not allow one to perform atomic relaxation. Moreover, at temperatures close to T_C, short range magnetic order, which is not taken into account in the CPA, can play an important role.

In this work, we calculate the solution energy of 3*p* (Al, Si) and 4*p* (Ga, Ge) elements in the ferromagnetic (FM) and paramagnetic (PM) states of iron with the use of both the DLM-CPA and the supercell method. We show that the allowance for the dependence of the solution energy on local magnetic polarization can lead to an increase in the solubility.

2. CALCULATION TECHNIQUE

The electronic structure and total energies calculations for the FM and PM states of the bcc iron alloyed by Al, Si, Ga, and Ge were performed using methods based on the density-functional theory (DFT) [31, 32] that were realized using the SIESTA [33] and LSGF [34, 35] packages. The use of these two approaches, which describe the paramagnetic state in different ways, permitted us to more precisely and reliably estimate the solution energy of the impurity in different magnetic states of the bcc iron.

The SIESTA package constructed on the basis of numerical atomic orbitals (NAO) was used to determine the local deformations and solution energies of impurity elements. The validity of applying this approach to iron alloys was considered in [36, 37], where it was shown that the reduction of the basis set for the 3*d* orbitals of Fe as compared to the usually employed DZ (double-ζ) and DZP (double ζ polarized) bases does not lead to a loss of accuracy, but makes it possible to spend less computational effort as compared to that required when using plane-wave basis. To describe valence electrons of Fe, we used the DZ basis for the 4*s* states and the SZ (single ζ) basis for the 4*p* and 3*d* states; the cut-off radius for the orbitals was taken to be 2.95 Å. For the impurity atoms, we used the standard DZP basis. The core electrons have been taken into account using a norm-conserving pseudopotential constructed using the Troullier–Martins scheme [38]. The nonlocal components of the pseudopotential are represented according to the Kleinman–Bylander scheme [39]. The exchange-correlation energy is taken into account in the generalized-gradient approximation (GGA) [40]. The cut-off energy E_{cutoff} was assumed to be 600 Ry. The integration over the Brillouin zone was replaced by summing over $6 \times 6 \times 6$ special **k** points chosen using the Monkhorst–Pack scheme [41].

The calculations were performed using a 54-atom supercell containing one impurity atom. In our previous work [42], it was shown that the use of an enhanced 128-atom supercell only insignificantly increases the accuracy of the calculation of the energies of solution. Upon calculating the ferromagnetic state, we performed a relaxation of the atomic positions and of the shape and volume of the cell; the accuracy of determining the magnitudes of the forces and of the total energy was 0.02eV/Å and 1 meV, respectively. In the paramagnetic case, the relaxation of atomic positions was performed at a fixed volume that was chosen based on the condition of the minimum of the total energy.

The method of locally self-consistent Green's functions (LSGF), which is based on the formalism of Green's functions [43, 44] and the coherent-potential approximation [45], was employed to calculate the energies of solution in both magnetic states of the bcc iron (FM and PM). The exchange-correlation energy was calculated in terms of the generalized-gradient approximation (GGA) [40]. The multipole correction of the atomic-sphere approximation (ASA + M) [46, 47] was used. The calculations were performed with the maximum orbital quantum number $l_{\max} = 3$. Correspondingly, the nonspherical charge density up to the moment $l = 6$ was taken into account in the electrostatic calculation of the energy. In the LSGF method, each atom of the supercell and its nearest neighborhood was considered self-consistently in the zone of local interaction embedded into an effective medium that retains the symmetry of the initial lattice. The solution energies of impurity elements in bcc iron were calculated using the LSGF method for a 54-atom cell at a fixed volume corresponding to experimental data for the ferromagnetic state of pure iron (2.86 Å) [48, 49] and for the paramagnetic state of iron with a lattice parameter equal to 2.90 Å [50]. The initial magnitudes of the magnetic moments were taken to be nonzero and could be changed in the process of the calculation.

The paramagnetic state in both methods was simulated in the approximation of disordered local moments (DLM). In this model, each site is assumed to be occupied with a 50% probability by Fe↑ (iron

with spin up) and by Fe↓ (iron with spin down). In [51], it was shown that the DLM configuration can be realized in a supercell with a distribution of magnetic moments such that the spin-correlation functions on the nearest coordination shells are equal to zero; in this case, the results obtained by this method agree quite well with the DLM-CPA calculations. This configuration, which is constructed using the method of distributions of special quasi-random structures (SQS) [52], corresponds to the model of an ideal paramagnetic state that is realized at temperatures $kT \gg J_0$, where J_0 is the magnitude of the exchange energy. On the other hand, it is known that the total energy determined as the average value over the ensemble of random magnetic configurations (magnetic sampling method (MSM)) [51] coincides with a good accuracy with the magnitude obtained when using the cell with an SQS distribution of magnetic moments. In order to clarify the role of short-range magnetic order upon the calculations by the SIESTA method, we used a set of cells with a random distribution of magnetic moments.

3. CALCULATION RESULTS

We have found that the lattice parameter of the FM bcc Fe after ionic relaxation is equal to 2.88 Å. This value agrees well with the experimental value a_{expt} = 2.86 Å [45] and with the preceding results obtained by the SIESTA method [33, 34]. The magnetic moment of Fe atom is 2.5 μB, which exceeds the values obtained by the techniques constructed on the plane-augmented waves (VASP) [53]. When calculating bcc Fe in the paramagnetic state, the lattice proved to be unstable and became transformed into the fcc lattice in the process of ionic relaxation. Therefore, the DLM calculations were performed at a fixed volume of a crystallite, which ensured the stability of the magnetic and crystal structures. Based on a series of DLM calculations, it was found that the minimum energy is obtained at the lattice parameter equal to 2.88 Å, which in the limits of error coincides with the a value of the bcc Fe calculated for the FM state. The same value was obtained in [54] in terms of the LDA + DMFT method. The difference in the energies between the FM and PM states of the bcc Fe is $E_{PM} - E_{FM} = -0.20$ eV/atom that is in a good agreement with the results of [52] where $E_{PM} - E_{FM} = -0.24$ eV/atom.

The substitution of an impurity atom for an iron atom leads to a local change in the electronic structure and in a displacement of nearest Fe atoms from the equilibrium positions in both the FM and PM states. Table 1 gives the local deformations for the ferromagnetic state of Fe–X alloys ($\varepsilon^{(1)}_{FM}$, $\varepsilon^{(2)}_{FM}$) [39], which represent relative changes in the distances between an impurity atom and the iron atoms on the first and second coordination shells (CSs) (the magnitude of the deformation was determined relative to the calculated value of the lattice parameter of the bcc Fe equal to 2.88 Å). The magnitudes of $\varepsilon^{(1)}_{PM}$ and $\varepsilon^{(2)}_{PM}$ were obtained by averaging the relative distances between the impurity atom and the iron atoms on the first and second CSs over all calculated magnetic configurations. It can be seen that the magnitudes of the local deformations change significantly upon the transition from the FM into the PM state on both the first and second CSs. As in the case of FM, the local deformations on both CSs increase with an increasing number of valence electrons in the impurity element (see Discussion in [39]). A special case is the Si impurity, which causes the largest deformations on both the first and second CSs. In contrast to the FM case, in the PM state the Fe atoms are displaced toward the impurity atom, which indicates a change in the relationship between the Fe–X and Fe–Fe bonds upon the transition from the FM into the PM state. As follows from a comparison of the E_{PM} and E_{FM} energies, there is a weakening of the Fe–Fe bond by ~0.03 eV, which leads to a large difference in the deformations $\varepsilon^{(1)}_{PM}$ and $\varepsilon^{(2)}_{PM}$. A weakening of this bond also follows from the magnitudes of the rms deviations (calculated in this work) of the positions of Fe atoms in pure bcc Fe from the crystallographic positions in the PM state, which reach approximately 2% for each coordinate.

Table 1. Relative changes in distances between the impurity atom X and Fe atoms on the first ($\varepsilon^{(1)}$) and second ($\varepsilon^{(2)}$) coordination shells (CSs) in the ferromagnetic (FM) and paramagnetic (PM) states of the bcc iron

Parameters	Al	Si	Ga	Ge
$\varepsilon^{(1)}_{FM}$, %	1.36	0.04	1.56	1.36
$\varepsilon^{(2)}_{FM}$, %	−0.69	−0.73	−0.24	−0.32
$\varepsilon^{(1)}_{PM}$, %	−8.2	−14.1	−7.9	−9.1
$\varepsilon^{(2)}_{PM}$, %	−1.0	−7.0	1.0	−2.3

The solution energy E_{sol} characterizes a change in the binding energy in the system upon the substitution of an impurity element for an iron atom. The magnitude of E_{sol} was determined as follows:

$$E_{sol} = [E_{tot}(Fe_N X_M) - NE_{tot}(Fe) - ME_{tot}(X)]/M, \quad (1)$$

where E_{tot} is the total energy of a cell with an impurity, E_{tot}(Fe) and E_{tot}(X) are the energies per atom in the ground structural state for the corresponding element, and M and N are the numbers of atoms of the corresponding elements. As can be seen from Table 2, in the FM state, the solution energy of substitutional impurities is negative and increases with impurity concen-

Table 2. Solution energy E_{sol} of alloying elements for different bcc-Fe-based superstructures in the ferromagnetic and paramagnetic states

Method (structure)	E_{sol} (Al), eV/atom	E_{sol} (Si), eV/atom	E_{sol} (Ga), eV/atom	E_{sol} (Ge), eV/atom
SIESTA ($B2$)	−0.66	−0.76	.0.04	0.12
SIESTA ($D0_3$)	−0.89	−1.18	−0.34	−0.54
SIESTA ($Fe_{53}X_1$) $a = 2.88$ Å FM	−1.02	−1.30	−0.48	−0.77
SIESTA ($Fe_{53}X_1$) $a = 2.86$ Å FM	−0.87	−1.20	−0.28	−0.59
LSGF ($Fe_{53}X_1$) $a = 2.86$ Å FM	−0.73	−0.94	−0.27	−0.35
SIESTA ($Fe_{53}X_1$) $a = 2.88$ Å DLM	−0.96	−1.25	−0.45	−0.69
LSGF ($Få_{53}X_1$) $a = 2.90$ Å DLM	−0.99	−1.02	−0.55	−0.59

tration. Since E_{sol}(Ga) and E_{sol}(Ge) become positive, in the case of the $B2$ ordering ($C_X = 50\%$), this superstructure does not appear in these alloys at temperatures below the Curie point T_C, in contrast to the Fe–Si and Fe–Al systems, where this phase coexists with the superstructure of the $D0_3$ type. The solution energy changes regularly depending on the principal quantum number and the number of valence electrons of the impurity atom. Silicon has the least solution energy in all configurations under consideration; this is explained by the specific features of p–d hybridization, as discussed in [39].

The solution energy of an impurity in the ferromagnetic state is sensitive to the choice of the lattice parameter. In the case of SIESTA calculations, the change in the lattice parameter from the equilibrium value $a_{calc} = 2.88$ Å to the experimental value $a_{expt} = 2.86$ Å, which was used in the LSGF approach, leads to an increase in the solution energy (ΔE_{sol}) from 0.1 eV (for Si) to 0.2 eV (for Ga). As can be seen from Table 2, the results of the SIESTA and LSGF calculations at the same lattice parameter prove to be close. The fixation of the atomic positions increases the solution energy of an impurity by no more than 0.1 eV. Therefore, the difference in the results cannot be explained by only the absence of the relaxation in the LSGF method but rather is due to the difference between the approximations employed.

Upon calculating the paramagnetic state of the bcc Fe using the SIESTA method, it turned out that the solution energy of an impurity depends substantially on its local magnetic neighborhood. To obtain a statistical description, we performed a series of calculations in which the impurity atom substituted for an Fe atom in different positions chosen in a random way. The distribution of the obtained energies of solution of an impurity X is shown in Fig. 1. An analysis of local magnetic configurations has shown that the highest and the lowest values of the solution energy correspond to the cases where magnetic moments of the same sense are predominant on the first CS of an impurity (states with a maximum magnetic polarization). The configurations without polarization in the first CS correspond to the total magnetic disordering near the impurity, which is assumed to take place in the CPA method. The distribution of the solution energies for such configurations is characterized by a dispersion that is two-times smaller relative to the average value (double hatching in Fig. 1).

The origin of the spread of the solution energies can be due to the difference in the local magnetic configurations in the neighborhood of the impurity. Indeed, the energy of configurations with maximum polarization can differ by $2\sum_i (\mathbf{e}_0 \cdot \mathbf{e}_i) J_{0i} \sim 2J_0$ ($J_0 = zJ_{0i}$ is the energy of exchange interaction of nearest neighbors of an Fe atom, where z is the number of nearest neighbors of the Fe atom; $\mathbf{e}_0$ and $\mathbf{e}_i$ are the unit vectors that determine the directions of the magnetic moments of Fe atoms) because of the different possible directions of the magnetic moment of the substituted Fe atom. In bcc Fe, the magnitude of $2J_0$ is approximately 0.4 eV [55], which leads to a significant dispersion of the solution energies. For the unpolarized configurations, the energy of exchange interaction is $J_0 = 0$ if the lengths of the magnetic moments are equal; therefore, the observed magnitude of the dispersion (double hatching in Fig. 1) is determined by the fluctuations of the length of the magnetic moment and by the difference in the local deformations of the first CS relative to the impurity in different magnetic configurations. Note that, in the case of DLM, the sensitivity of the solution energy to the change in the lattice parameter proved to be substantially less than that in the FM case (the change in E_{sol} is less than 0.1 eV); therefore, when calculating this energy, we restricted ourselves to the use of statistics with an equilibrium lattice parameter $a = 2.88$ Å.

Table 2 contains the solution energies obtained by averaging over configurations with an unpolarized

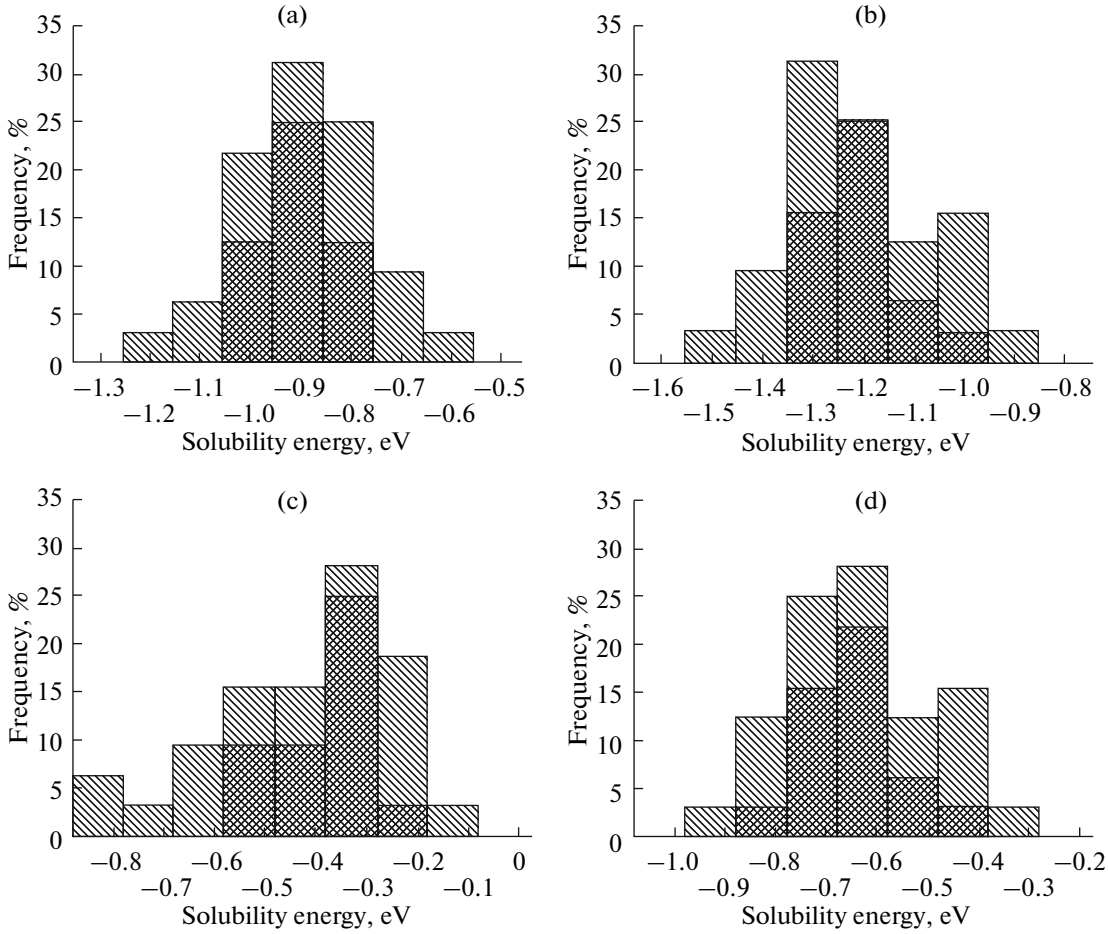

Fig. 1. Distribution of the solution energy E_{sol} of an impurity for a sampling of unpolarized (double hatching) and partly polarized (simple hatching) calculated magnetic configurations for the systems studied: (a) Fe–Al; (b) Fe–Si; (c) Fe–Ga; and (d) Fe–Ge.

local magnetic neighborhood of the impurity. In spite of the difference in the approximations used in the SIESTA and LSGF methods, the results proved to be close. This coincidence can partly be explained by a small contribution of the energy of rela xation to the solution energy in the DLM state, which is less than 0.1 eV. Therefore, the absence of relaxation in the LSGF method do not produce the significant error in the solution energy calculations. It should be noted that, in the case of DLM, the fixation of the atomic positions also leads to the fixation of magnetic moments. At the same time, in contrast to the FM state, in the case of DLM the relaxation of all atomic positions in the crystallite occurs, which can be seen from the large value of rms deviation.

4. DISCUSSSION

It can be seen from Table 2 that the regular variation of the solution energy of an impurity depending on its position in the Periodic Table for the case of FM ordering, which was discussed in our previous work [42], is retained in the PM state as well. This means that the solubility is determined by the properties of the Fe–X chemical bonds, which do not change qualitatively upon the transition into the paramagnetic state. At the same time, the weakening of the Fe–Fe bonds occurs, which follows from the increase in the energy of Fe upon the transition into the paramagnetic state. This in turn leads to a significant increase in local deformations near the impurity atom (Table 1). Nevertheless, the results of calculations using the SIESTA and LSGF methods turned out to be close, which is due to the small contribution from the energy of relaxation to E_{sol}. Thus, the LSGF method can lead to an overestimation of the E_{sol} values, but the error introduced is small.

When using the equilibrium lattice parameter, the magnitude of E_{sol} is virtually independent of the magnetic state of the alloy. However, in the calculations with the use of the experimental lattice parameter, in all the alloys under consideration there occurs a decrease in the magnitude of E_{sol} upon the transition from the FM into the PM state, which is especially pronounced for Ga. Thus, as the temperature

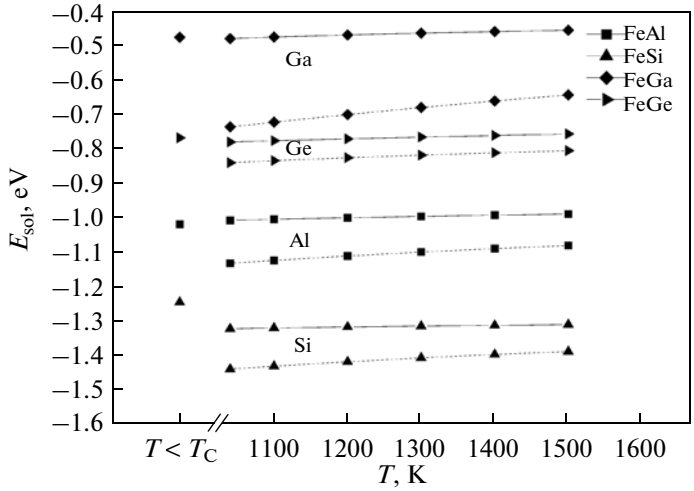

Fig. 2. Temperature dependence of solution energies of unpolarized (solid lines) and partly polarized (dashed lines) magnetic configurations. At $T < T_C$, solution energies of the impurity in the ferromagnetic state of the bcc Fe are shown.

increases to above T_C, we should expect an increase in the solubility of the impurities under study.

Note that the magnitude of E_{sol} in the case of FM is more sensitive to the change in the lattice parameter than in the PM case. This is due to the fact that the density of states of the ferromagnetic iron has a more pronounced peaked character; therefore, even a small change in the lattice parameter can exert a strong effect on the density of states near the Fermi level and, consequently, on the character of the Fe–X chemical bonds.

The above-given values of the solution energy of impurities have been obtained by averaging over a sampling of magnetic configurations without polarization in the first coordination shell. This approach corresponds to the approximation employed in the CPA and is valid for high temperatures ($T \gg T_C$) when the different magnetic configurations are encountered with identical weights. Short-range magnetic order appears in the temperature interval close to Curie temperature ($T > T_C$), which results in increasing of weight of low energy configurations when averaging in accordance with Boltzmann law. As can be seen from Fig. 1, the polarized configurations can possess a lower energy, which in turn leads to a decrease in the average value of the solution energy as the temperature decreases.

To estimate the effect of the short-range magnetic order on the solution energy, we used Eq. (1) in which E_{tot} was specified as

$$E_{tot} = \sum_i E_i \exp\left(-\frac{E_i}{kT}\right)/Z, \qquad (2)$$

where $Z = \sum_i \exp\left(-\frac{E_i}{kT}\right)$, and the summation was implemented over configurations with the energies E_i. The energies of solution that were obtained by Eqs. (1) and (2) as functions of T are given in Fig. 2. The calculated temperature range lies above T_C for pure iron (~1040 K) and corresponds to the technologically important temperatures of iron alloys. At $T < T_C$, the solution energy of impurities in ferromagnetic bcc Fe is given in Fig. 2. It can be seen that, when taking into account only unpolarized magnetic configurations, E_{sol} is almost independent of T. The allowance for the polarized configurations leads to a significant decrease in E_{sol} in the temperature range corresponding to the paramagnetic bcc Fe, especially at temperatures close to T_C.

It can be seen from Fig. 2 that the largest decrease in E_{sol} upon allowance for short-range magnetic order occurs in the Fe–Ga system. This is due to the existence of low values of E_{sol} for the polarized configurations in the distribution given in Fig. 1. Although the decrease in E_{sol} for the other systems does not exceed 0.1 eV, we should expect the appearance of a singularity in the behavior of the solubility at the Curie point. However, in the phase diagram of these alloys the limit of solubility is preceded by a two-phase field, in which a short-range order of the $B2$ or $D0_3$ type is realized. The formation of this or that short-range order is determined by the energy of pairwise effective interaction of impurities. As was shown in [4] for Fe–Si, this energy and, correspondingly, the type of short-range order change upon the transition from the FM into the PM state. The allowance for the magnetic polarization in a vicinity of an impurity can affect the energy of interaction and thereby enhance the difference in the behavior of the alloys in the temperature range above and below T_C.

5. CONCLUSIONS

Thus, the use of two methods (SIESTA and LSGF) of calculating the solution energy in the paramagnetic state made it possible to obtain reliable results and to clarify the advantages and disadvantages of the approximations employed. It has been found that the energies of solution obtained in terms of the supercell DLM approach (SIESTA), which takes into account only the unpolarized magnetic configurations, agree well with the LSGF results. Although the local deformations in the DLM approximation proved to be significant in the vicinity of the impurity, the contribution from the atomic relaxation to the energy of solution is small. At the same time, the allowance for polarized magnetic configurations can lead to a decrease in E_{sol}, which is especially strongly pronounced at $T \sim T_C$ in the Fe–Ga alloy. Since, in the approach used in our work, it is assumed that the magnetic subsystem is slower than the lattice subsystem (static DLM), this approach can overestimate the magnitude of the atomic relaxation and the contribution from the local magnetic polarization to the solution energy. Nevertheless, we believe that the results obtained in this work are valid qualitatively.

ACNOWLEDGMENTS

This work was supported by the Russian Foundation for Basic Research (project no. 10-02-100435) and by the Presidium of the Russian Academy of Sciences (project no. 12-P-23-2005). The results of the work were obtained using computational resources of MCC NRC "urchatov Institute" (http://computing.kiae.ru/).

REFERENCES

1. Y. Yoshizawa, S. Oguma, and K. Yamauchi, "New Fe-based soft magnetic alloys composed of ultrafine grain structure," J. Appl. Phys. **64**, 6044–6046 (1988).
2. B. Hofman and H. Kronmüller, "Stress-induced magnetic anisotropy in nanocrystalline FeCuNbSiB alloy," J. Magn. Magn. Mater. **152**, 91–98 (1996).
3. A. R. Kuznetsov, Yu. N. Gornostyrev, N. V. Ershov, V. A. Lukshina, Yu. P. Chernenko, and V. I. Fedorov, "Atomic displacements and short-range order in the FeSi soft magnetic alloys: Experiment and ab initio calculations," Phys. Solid State **49**, 2290–22297 (2007).
4. O. I. Gorbatov, A. R. Kuznetsov, and Yu. N. Gornostyrev, A. V. Ruban, N. V. Ershov, V. A. Lukshina, Yu. P. Chernenko, and V. I. Fedorov, "Role of magnetism in the formation of a short-range order in iron–silicon alloys," J. Exper. Theor. Phys. **112**, 848–859 (2011).
5. A. E. Clark, K. B. Hathaway, M. Wun-Fogle, J. B. Restorff, T. A. Lograsso, V. M. Keppens, G. Petculescu, and R. A. Taylor, "Extraordinary magnetoelasticity and lattice softening in bcc Fe–Ga alloys," J. Appl. Phys. **93**, 8621–8623 (2003).
6. J. Restorff, M. Wun-Fogle, K. B. Hathaway, A. E. Clark, T. A. Lograsso, and G. Petculescu, "Tetragonal magnetostriction and magnetoelastic coupling in Fe–Al, Fe–Ga, Fe–Ge, Fe–Si, Fe–Ga–Al and Fe–Ga–Ge alloys," J. Appl. Phys. **111**, 023905 (2012).
7. E. M. Summers, T. A. Lograsso, and M. Wun-Fogle, "Magnetostriction of binary and ternary Fe–Ga alloys," J. Mater. Sci. **42**, 9582–9594 (2007).
8. R. Wu, "Origin of large magnetostriction in FeGa alloys," J. Appl. Phys. **91**, 7358–7360 (2002).
9. J. Boisse, H. Zapolsky, and A. G. Khachaturyan, "Atomic scale modeling of nanostructure formation in Fe–Ga alloys with giant magnetostriction: Cascade ordering and decomposition," Acta Mater. **59**, 2656–2668 (2011).
10. O. I. Gorbatov, Y. N. Gornostyrev, A. R. Kuznetsov, and A. V. Ruban, "Effect of magnetism on short-range order formation in Fe–Si and Fe–Al alloys," Solid State Phenom. **172–174**, 618–623 (2011).
11. Y. Du, M. Huang, S. Chang, D. L. Schlagel, T. A. Lograsso, and R. J. McQueeney, "Relation between Ga ordering and magnetostriction of Fe–Ga alloys studied by X-ray diffuse scattering," Phys. Rev. B: Condens. Matter Mater. Phys. **81**, 054432 (2010).
12. P. Olsson, T. P. C. Klaver, and C. Domain, "Ab initio study of solute transition-metal interactions with point defects in bcc Fe," Phys. Rev. B: Condens. Matter Mater. Phys. **81**, 054102 (2010).
13. G. Rahman, I. G. Kim, H. K. D. H. Bhadeshia, and A. J. Freeman, "First-principles investigation of magnetism and electronic structures of substitutional 3*d* transition-metal impurities in bcc Fe," Phys. Rev. B: Condens. Matter Mater. Phys. **81**, 184423 (2010).
14. B. Drittler, N. Stefanou, S. Blügel, R. Zeller, and P. H. Dederichs, "Electronic structure and magnetic properties of dilute Fe alloys with transition-metal impurities," Phys. Rev. B: Condens. Matter **40**, 8203–8212 (1989).
15. W. Liu, W.-L. Wang, Q. F. Fang, C. S. Liu, Q.-Y. Huang, and Y.-C Wu, "Concise relation of substitution energy to macroscopic deformation in a deformed system," Phys. Rev. B: Condens. Matter Mater. Phys. **84**, 224101 (2011).
16. A. P. Miodownik, "The effect of magnetic transformations on phase diagrams," Bull. Alloy Phase Diagrams **2**, 406–412 (1982).
17. G. Inden, "The effect of continuous transformations on phase diagrams," Bull. Alloy Phase Diagrams **2**, 412–422 (1982).
18. C. Zener, "Impact of magnetism upon metallurgy," Trans. AIME **203**, 619–630 (1955).
19. L. Kaufman, E. V. Clougherty, and R. J. Weiss, "The lattice stability of metals—III. Iron," Acta Metall. **11**, 323–335 (1963).
20. M. Hillert, T. Wada, and H. Wada, "The α–γ Equilibrium in Fe–Mn, Fe–Mo, Fe–Ni, Fe–Sb, Fe–Sn and Fe–W systems," J. Iron Steel Inst. **205**, 539–546 (1967).
21. M. Hillert and M. Jarl, "A model for alloying effects in paramagnetic metals," Calphad **2**, 227–238 (1978).
22. A. V. Ruban, P. A. Korzhavyi, and B. Johansson, "First-principles theory of magnetically driven anoma-

lous ordering in bcc Fe–Cr alloys," Phys. Rev. B: Condens. Matter Mater. Phys. **77**, 094436 (2008).

23. P. A. Korzhavyi, A. V. Ruban, J. Odqvist, et al., "Electronic structure and effective chemical and magnetic exchange interactions in bcc Fe–Cr alloys," Phys. Rev. B: Condens. Matter Mater. Phys. **79**, 054202 (2009).
24. O. I. Gorbatov, A. V. Ruban, P. A. Korzhavyi, and Yu. N. Gornostyrev, "Effect of magnetism on precipitation of Cu in bcc Fe," Mater. Res. Soc. Symp. Proc. **1193**, 469–476 (2009).
25. W. Metzner and D. Vollhardt, "Correlated lattice fermions in $d = \infty$ dimensions," Phys. Rev. Lett. **62**, 324–327 (1989).
26. G. Kotliar and D. Vollhardt, "Strongly correlated materials: Insights from dynamical mean-field theory," Phys. Today **57**, 53–59 (2004).
27. M. Cyrot, "Phase transition in Hubbard model," Phys. Rev. Lett. **25**, 871–874 (1996).
28. J. Hubbard, "Magnetism of iron," Phys. Rev. B: Condens. Matter **20**, 4584–4595 (1979).
29. B. L. Gyorffy, A. J. Pindor, J. B. Stauton, G. M. Stocks, and H. Winter, "A first-principles theory of ferromagnetic phase transitions in metals," J. Phys. F: Met. Phys. **15**, 1337–1386 (1985).
30. A. V. Ruban and V. I. Razumovskiy, "Spin-wave method for the total energy of paramagnetic state," Phys. Rev. B: Condens. Matter Mater. Phys. **85**, 174407 (2012).
31. P. Hohenberg and W. Kohn, "Inhomogeneous electron gas," Phys. Rev. B: **136**, 864–871 (1964).
32. W. Kohn and L. J. Sham, "Self-consistent equations including exchange and correlation effects," Phys. Rev. A **140**, 1133–1138 (1965).
33. J. M. Soler, E. Artacho, J. D. Gale, A. Garcia, J. Junquera, P. Ordejón, and D. Sanchez-Portal, "The SIESTA method for ab initio order-N materials simulation," J. Phys.: Condens. Matter **14**, 2745–2779 (2002).
34. I. A. Abrikosov, A. M. N. Niklasson, S. I. Simak, B. Johansson, A.V. Ruban, and H. L. Skriver, "Order-N Green's function technique for local environment effects in alloys," Phys. Rev. Lett. **76**, 4203–4206 (1996).
35. I. A. Abrikosov, S. I. Simak, A. V. Ruban, and H. L. Skriver, "Locally self-consistent Green's function approach to the electronic structure problem," Phys. Rev. B: Condens. Matter **56**, 9319–9334 (1997).
36. R. Soulairol, C. C. Fu, and C. Barreteau, "Structure and magnetism of bulk Fe and Cr: From plane waves to LCAO methods," J. Phys.: Condens. Matter **22**, 295502 (2010).
37. C. C. Fu, F. Willaime, and P. Ordejon, "Stability and mobility of mono- and di-interstitials in α-Fe," Phys. Rev. Lett. **92**, 175503 (2004).
38. N. Troullier and J. L. Martins, "Efficient pseudopotentials for plane-wave calculations," Phys. Rev. B: Condens. Matter **43**, 1993–2006 (1991).
39. L. Kleinman and D. M. Bylander, "Efficacious form for model pseudopotentials," Phys. Rev. Lett. **48**, 1425–1428 (1982).
40. J. P. Perdew, K. Burke, and M. Ernzerhof, "Generalized gradient approximation made simple," Phys. Rev. Lett. **77**, 3865–3568 (1996).
41. H. J. Monkhorst and J. D. Pack, "Special points for Brillouin-zone integrations," Phys. Rev. B: Solid State **13**, 5188 (1976).
42. M. V. Petrik and Yu. N. Gornostyrev, "Local deformations and chemical bonding in "Fe–X (X = Si, Al, Ga, Ge)," Phys. Met. Metallogr. **114**, 469–473 (2013).
43. J. Korringa, "On the calculation of the energy of a Bloch wave in a metal," Physica **13**, 392–400 (1947).
44. W. Kohn and N. Rostocker, "Solution of the Schrödinger equation in periodic lattices with an application to metallic lithium," Phys. Rev. **94**, 1111–1120 (1954).
45. P. Soven, "Coherent-potential model of substitutional disordered alloys," Phys. Rev. **156**, 809–813 (1967).
46. H. L. Skriver and N. M. Rosengaard, "Self-consistent Green's-function technique for surfaces and interfaces," Phys. Rev. B: Condens. Matter **43**, 9538–9549 (1991).
47. P. A. Korzhavyi, I. A. Abrikosov, A. V. Ruban, and H. L. Skriver, "First-principles calculations of the vacancy formation energy in transition and noble metals," Phys. Rev. B: Condens. Matter Mater. Phys. **59**, 11693–11703 (1999).
48. Z. S. Basinski, W. Hume-Rothery, and A. L. Sutton, *Proc. R. Soc. A (London)*, **229**, 459–467 (1955).
49. I. Seki and K. Nagata, "Lattice constant of iron and austenite including its supersaturation phase of carbon," ISIJ Int. **45**, 1789–1794 (2005).
50. R. W. G. Wyckoff, *Crystal Structures* (Interscience, New York, 1963).
51. B. Alling, T. Marten, and I. A. Abrikosov, "Effect of magnetic disorder and strong electron correlations on the thermodynamics of CrN," Phys. Rev. B: Condens. Matter Mater. Phys. **82**, 184430 (2010).
52. A. Zunger, S.-H. Wei, L. G. Ferreira, and J. E. Bernard, "Special quasirandom structures," Phys. Rev. Lett. **65**, 353–356 (1990).
53. S. V. Okatov, Yu. N. Gornostyrev, A. I. Lichtenstein, and M. I. Katsnelson, "Magnetoelastic coupling in γ-iron investigated within an ab initio spin spiral approach," Phys. Rev. B: Condens. Matter Mater. Phys. **84**, 214422 (2011).
54. I. Leonov, A. I. Poteryaev, V. I. Anisimov, and D. Vollhardt, "Electronic correlations at the α–γ structural phase transition in paramagnetic iron," Phys. Rev. Lett. **106**, 106405 (2011).
55. S. V. Okatov, A. R. Kuznetsov, Yu. N. Gomostyrev, V. N. Urtsev, and M. I. Katsnelson, "Effect of magnetic state on the γ–α transition in iron: First-principles calculations of the Bain transformation path," Phys. Rev. B: Condens. Matter Mater. Phys. **79**, 094111 (2009).

Translated by S. Gorin